

A STUDY OF PILE-UP IN 200 GEV AU+AU COLLISIONS AT RHIC

BY

IAN HARNARINE
B.Sc. (York University) 2002

THESIS

Submitted in partial fulfillment of the requirements
for the degree of Master of Science in Physics
in the Graduate College of the
University of Illinois at Chicago, 2005

Chicago, Illinois

Copyright by

Ian Harnarine

2005

To my family,

Dhanidath, Linda and Wendy Harnarine,

for a lifetime of love, selflessness and support.

ACKNOWLEDGMENTS

I am deeply indebted to the members of my committee who are David Hofman, Russell Betts and Richard Hollis. Dave has been a continuous supply of guidance, patience, kindness and friendship over the years. I must thank Dave and Russell for believing in me from the start, and always being supportive in my endeavors. Richard suggested this study and has always dropped his own work to answer my questions. He also painstakingly read through each draft of this thesis and provided useful comments. Thank you.

I must thank Vasundhara Chetluru, Edmundo Garcia-Solis, Aneta Iordanova, Joseph Sagerer and Chadd Smith for useful comments and always answering my questions. It has been an honor to learn from them. I am also grateful for their friendship and being my partners in crime.

I would like to personally acknowledge Sohail Bastani, Ira Kosloff, Craig Lennon, Nadia & the Mohammed family, Roy Nyberg, Nidhi Patel, Ernest Robinson, Devon-Marie Shepherd (here's to never settling!), Elena Stevanato (good food/fun), Paul Tumaneng and Jerome Whyte. I am a better person for knowing them.

I am grateful to the Department of Physics and to UIC for partial funding during my studies. This work was partially supported by U.S. DOE grants DE-AC02-98CH10886, DE-FG02-93ER40802, DE-FC02-94ER40818, DE-FG02-94ER40865, DE-FG02-99ER41099, and W-31-109-ENG-38, by U.S. NSF grants 9603486, 0072204, and 0245011, by Polish KBN grant 1-P03B-062-27(2004-2007), by NSC of Taiwan Contract NSC 89-2112-M-008-024, and by Hungarian OTKA grant (F 049823).

TABLE OF CONTENTS

<u>CHAPTER</u>		<u>PAGE</u>
1	INTRODUCTION	1
1.1	Goals	1
1.2	Overview of RHIC	1
1.3	The PHOBOS Experiment	2
1.4	The PHOBOS Detector	3
1.4.1	PHOBOS Detector Overview	4
1.4.2	Octagon Silicon Detector	7
1.4.3	Silicon Ring Detector	8
1.4.4	Paddle Trigger Counters	12
2	PILE-UP	13
2.1	What is Pile-up?	13
2.1.1	The Importance to PHOBOS	13
2.1.2	Pre-Pile-Up	14
2.1.3	Post-Pile-Up	16
2.2	Pile-Up Trigger Logic	16
2.2.1	Pre-Pile-up Trigger Logic	16
2.2.1.1	Previous Event Processing	18
2.2.1.2	Current Event Processing	18
2.2.1.3	Pre-Pile-up Decision	20
2.2.2	Post-Pile-up Trigger Logic	20
2.2.2.1	Current Event Processing	22
2.2.2.2	Next Event Processing	24
2.2.2.3	Post-Pile-up Decision	24
2.3	Effects of Pileup on Detectors	24
2.3.1	Paddle Detectors	24
2.3.2	Octagon	25
2.3.3	Rings	26
3	STUDY OF PILE-UP	27
3.1	Rationale	27
3.2	Data Used	28
3.2.1	Problem with Statistics	29
3.3	Study of Pile-up with Paddle Detector	31
3.3.1	The Effect of Pile-up on MIP signals	31
3.3.2	The Effect of Pile-up on Centrality	32
3.4	Paddles Summary	36

TABLE OF CONTENTS (Continued)

<u>CHAPTER</u>		<u>PAGE</u>
3.5	Study of Pile-up with Octagon Detector	36
3.6	Study of Pile-up with Ring Detector	38
3.7	Summary of Octagon and Ring Detectors	39
4	CONCLUSION	40
	APPENDICES	41
	Appendix A	42
	Appendix B	43
	CITED LITERATURE	44
	VITA	45

LIST OF TABLES

<u>TABLE</u>		<u>PAGE</u>
I	THE RUNS USED IN THIS STUDY WITH AMOUNT OF NO PILEUP EVENTS, PILE-UP EVENTS AND THE RATIO (PILE-UP/NO PILE-UP).	30
II	AN EXAMPLE OF THE MEAN AND SIGMA VALUES WITH ASSOCIATED ERRORS EXTRACTED FROM THE GAUSSIAN FITS FOR THE TOP NINE CENTRALITY BINS.	34

LIST OF FIGURES

<u>FIGURE</u>		<u>PAGE</u>
1	The RHIC Complex	2
2	The PHOBOS Detector	5
3	The Octagon and Ring Detectors	8
4	The Octagon Detector Signal	9
5	The Silicon Pad Layouts	10
6	The Signal From a Ring	11
7	Schematic Illustration of Pile-up	15
8	The Pre-Pile-up Trigger Logic	17
9	Details of the Pre-Pile-up Logic	19
10	The Pre-Pile-up Trigger Logic	21
11	Details of the Post-Pile-up Logic	23
12	Signal Rise and Fall Time for the Paddle Detector	25
13	Signal Rise and Fall Time for Silicon Detector	26
14	Ratio of Pile-up/No-Pile-up Correlated with Run #	28
15	The MIP signals from the Paddles with pile-up and without pile-up. . .	31
16	The Paddle Mean Distribution with and without pile-up.	32
17	EOct Cutting on Paddle Mean Signal for a Given Centrality	33
18	The Percent Differences of PdlMean Mean and Sigma values for pile-up and no pile-up events.	35

LIST OF FIGURES (Continued)

<u>FIGURE</u>		<u>PAGE</u>
19	EOct Signal with Paddle Mean Signal	36
20	The Percent Differences of PdlMean Mean and Sigma values for pile-up and no pile-up events.	37
21	The Percent Differences of PdlMean Mean and Sigma values for pile-up and no pile-up events.	38
22	The PHOBOS Trigger Diagram	43

LIST OF ABBREVIATIONS

BNL	Brookhaven National Laboratory
FO	Fan Out
GDG	Gate Delay Generator
L0	Level Zero Trigger
L1	Level One Trigger
RHIC	Relativistic Heavy Ion Collider
MIP	Minimum Ionizing Particle
QCD	Quantum Chromo Dynamics
QGP	Quark-Gluon Plasma
TOF	Time Of Flight
T0	Time-zero Čerenkov Detector
UIC	University of Illinois at Chicago
ZDC	Zero-Degree Calorimeter

SUMMARY

Particles depositing energy into detectors form the basis for measurements in experimental nuclear physics. It is the precise measurement of this energy that leads to measurements such as multiplicity, centrality and flow. Experimental effects, such as multiple collisions during the read-out of detectors can adversely increase the amount of energy deposited. This effect, known as *Pile-up*, is a potentially serious problem, as it increases the amount of background signal, thus giving unreliable measurements. This Thesis presents a study of the effects of pile-up in $Au + Au$ collisions at 200 GeV.

Results of this study indicate that only the lowest part of the energy spectrum of the Paddle detectors are affected. These effects are not large enough to manifest themselves in the centrality measurements and subsequent multiplicity measurements. Small pile-up effects were determined to exist in the Octagon and Ring silicon detectors. These effects are not statistically significant.

CHAPTER 1

INTRODUCTION

1.1 Goals

A study of pile-up and how the PHOBOS hardware measures it is presented. The main goal of this Thesis is to investigate the effect of pile-up in three PHOBOS detectors and its possible effect on measured PHOBOS variables.

1.2 Overview of RHIC

The Standard Model developed in the 1970's, describes the fundamental building blocks of matter and the interactions between them. According to theory, the strong force, mediated through gluons, binds the quarks together into nuclei and atoms. The Relativistic Heavy Ion Collider (RHIC) at Brookhaven National Laboratory was completed in 1999 and began taking data in 2000 as the world's largest heavy ion collider. By providing collisions of p+p, Au+Au, d+Au and most recently Cu+Cu, RHIC has created the highest energy densities produced in a controlled laboratory environment. At such large center-of-mass energies (e.g. $\sqrt{s_{NN}}=200$ GeV) it is theorized, by quantum chromodynamics (QCD), that a state of deconfined quarks and gluons, the Quark-Gluon Plasma (QGP), may be formed. It is generally accepted that several signatures of this state must coincide, over many events, for the QGP to be confirmed.

There are four complementary experiments at RHIC: PHOBOS, STAR, PHENIX and BRAHMS.

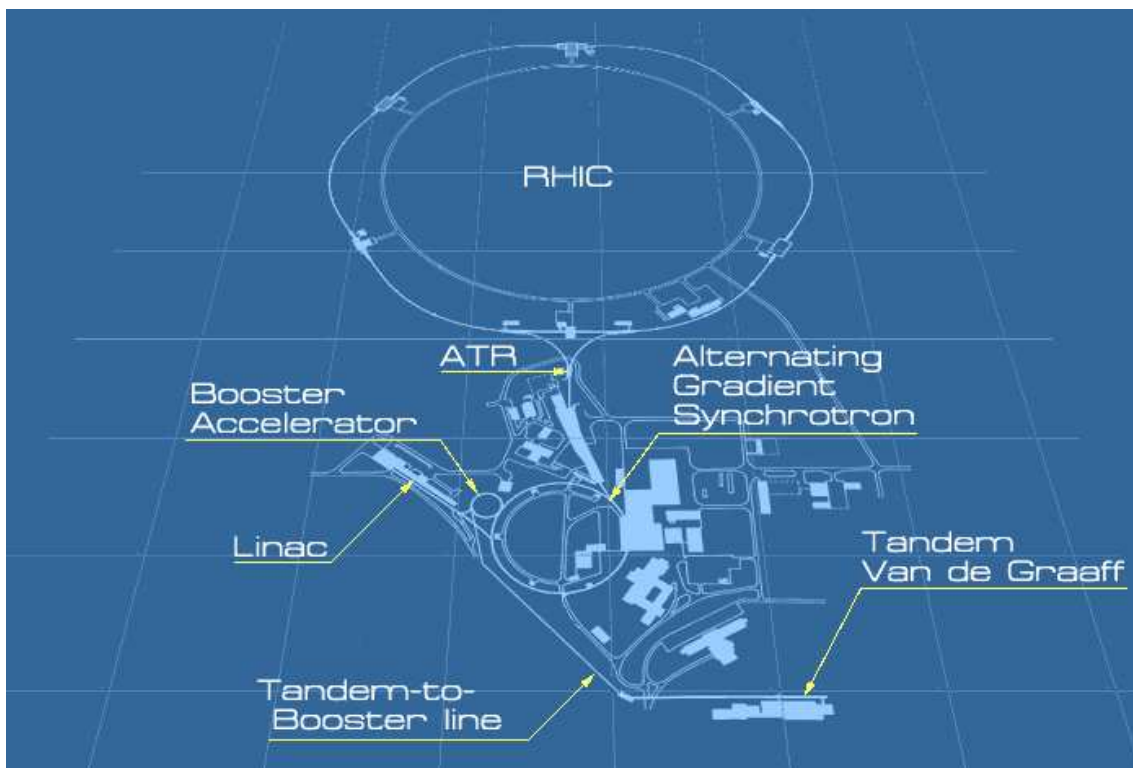


Figure 1. The Relativistic Heavy Ion Collider at Brookhaven National Laboratory. PHOBOS is located at the 10 o'clock point.

1.3 The PHOBOS Experiment

The PHOBOS experiment is located at the 10 o'clock position around the RHIC ring. The PHOBOS collaboration is made up of 12 institutions from 3 countries (see Appendix A).

The goal of the PHOBOS experiment is to observe the expected signatures of the QGP by measuring and analyzing hadronic observables over a large number of events. With such a large number of events being produced, PHOBOS is concerned with correctly identifying

and studying the most interesting heavy-ion collisions. For each collision, PHOBOS is able to make a global observation of all the charged particles produced in the collision with more detailed information about a subset in the region of highest particle yield. With this knowledge, PHOBOS hopes to detect and study the phase transition between ordinary (hadronic) matter and the QGP which will lead to a greater understanding of the early universe.

1.4 The PHOBOS Detector

There are several factors that were considered when constructing the detectors for PHOBOS.

1. The high density of produced particles.
 - The sheer number of charged particles produced in a single collision, with the analogous charged particle densities, place limitations on the materials used.
2. The large range of pseudo-rapidity, η .
 - Any indication of new physics could be from signatures that are extremely rare. Thus, data taken over a large area of pseudo-rapidity (a measurement of angle), η increases the global information for a collision.
3. The large range of transverse momentum, p_t .
 - By being able to measure a large range of p_t , PHOBOS is able to search for signatures of the QGP: for example, an increase in the amount of charged particles produced at low p_t .
4. The high rate of data collection.

- The ability to record data at high rates allows for sufficient statistics to search for rare, unusual events or fluctuations (indicators of new physics) offline.

5. Low production of background particles.

- PHOBOS utilizes a 1 mm thick Beryllium beam pipe. It serves many important purposes such as the minimization of energy loss, multiple scattering and secondary production of low p_t particles (which could be the cause of a background particles). The thickness of the Beryllium beam pipe is also responsible for setting the minimum p_t of detectable particles (10 MeV/c) and for the total momentum of particles (30 MeV/c).

Physically, the PHOBOS detector is comprised of four elements: several trigger detectors, which can be used to measure the centrality of collisions, a 4π multiplicity array, two-arm magnetic spectrometer for the tracking of charged particles and also a time-of-flight wall to help identify the charged particles. These are illustrated in Figure 2.

By matter of convention, the PHOBOS coordinate system is a right handed system defined with respect to the interaction point. The z -axis is along the beam, the $+y$ -axis is in the vertical direction and the $+x$ -axis is defined as the horizontal plane on the side of the TOF-wall.

1.4.1 PHOBOS Detector Overview

The angular distribution and the number of charged particles from a collision is measured (in the range of $|\eta| \leq 5.4$) using the Multiplicity Array. The region of $|\eta| < 3.2$ is covered by silicon detectors in an octagonal-barrel shape. Six silicon ring detectors ($3.0 \leq |\eta| \leq 5.4$) are

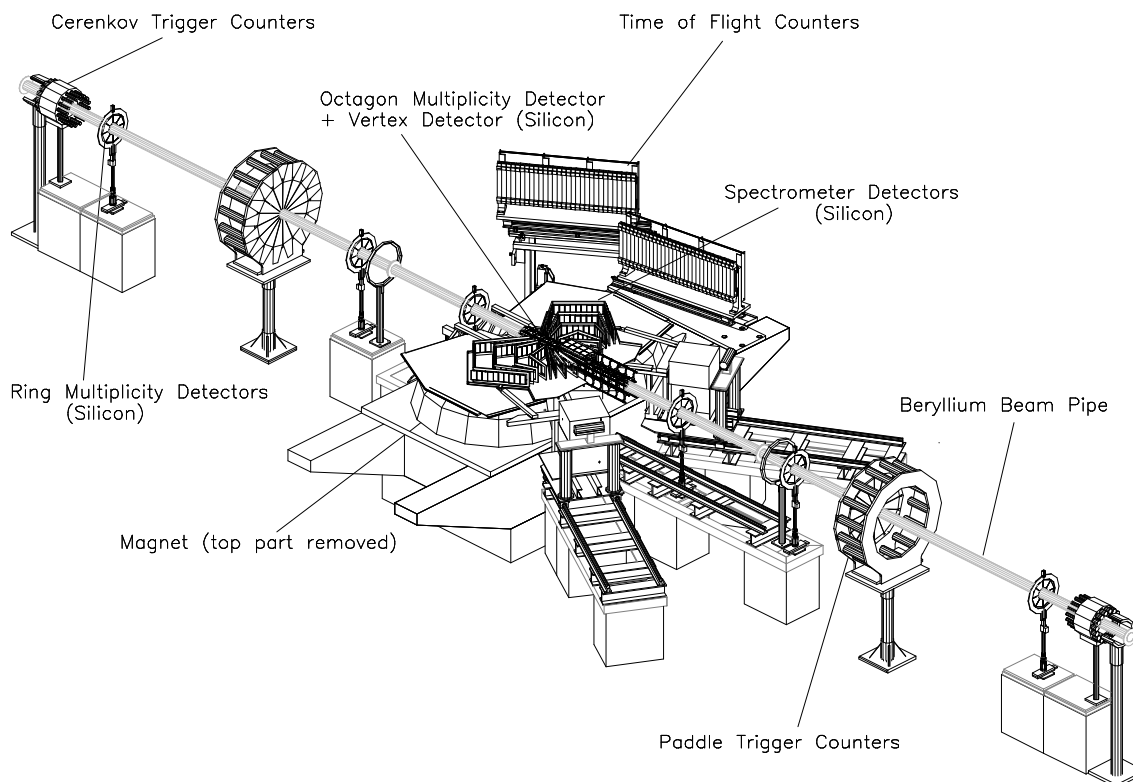


Figure 2. Schematic diagram of the PHOBOS detector for the PR01 set-up. The top yoke of the magnet is removed.

located at ± 1.13 m, ± 2.35 m and ± 5.05 m with respect to the interaction point along the z -axis.

The location of the collision vertex is reconstructed using finely segmented silicon sensors placed in two layers both above and below the nominal interaction point (covering $|\eta| \leq 1.0$).

Each side of the beam axis contains one arm of the dual-arm Spectrometer, with each arm comprised of fifteen Silicon layers. The total coverage of this detector is $0.8 < \eta < 1.4$. The η and ϕ -coverage of the spectrometer allows for about 2% of the charged particles in any given collision being identified (by measuring the Energy Loss, dE/dx , and momentum in each Silicon layer) and tracked. The particle identification abilities can be increased to include higher p_t particles by the inclusion of two arrays of scintillator material that make up the time-of-flight (TOF) counters.

PHOBOS uses a room-temperature double dipole magnet which creates opposing field directions on the two sides. The Spectrometer is placed such that the majority of the planes are subjected to a constant 2 T vertical field. However, there are a few parts of the spectrometer, near the nominal interaction point, that are subjected to smaller magnetic fields, and the straight tracks obtained in this region serve as a starting point to reconstruct the curved paths that occur in the higher magnetic field regions.

The timing coincidence of two sets of 16 scintillator Paddle counters that are located at $z = \pm 3.21$ m ($3.2 < |\eta| < 4.5$) determine the event trigger. The Paddle detectors ensure that only collisions that occur close to the center of the interaction region are considered. 16 Čerenkov detectors located near to each end of the Beryllium beam pipe provide additional triggering and collision vertex determination.

The Zero-degree calorimeters (ZDC), located at $z = \pm 18.5$ m from the interaction point, provide another means to ascertain luminosity and centrality.

For this analysis, three subsystems were used: the Octagon and Ring silicon detectors and the Paddle Trigger detector. These detectors were chosen for study as the effect of pileup is expected to be most apparent.

1.4.2 Octagon Silicon Detector

The Octagon detector is composed of 92 silicon pad detectors mounted on 8 faces. There is a maximum of 13 sensors on each face and they are arranged such that each face is opposite another to form an octagonal barrel shape with a mean diameter of 90 mm and a total length of 1.10 m. Each sensor is 36 mm in width and 84 mm in length. The active area of each sensor has 30 x 4 silicon pads, arranged with the four rows along the z direction. In order to not hinder the acceptance of other detectors (namely the vertex and spectrometer detectors), there is a void in the Octagon's acceptance in the region closest to the interaction region.

The configuration allows for a very simple read-out system so that each pad on a sensor is handled by one 128-channel preamplifier. The preamplifier also devotes some channels to monitoring noise and baseline response. This pad arrangement was chosen to minimize the complexity of the read-out, optimize the expected occupancy and to maximize η coverage.

An important feature of the Octagon is the aluminum support structure which partly contains Aluminum tubes filled with circulating cold water to cool down the read-out electronics attached to the sensors. The support structure occupies very little space in the interaction region which limits the possibility of secondary particle production and multiple scattering. The light-weight yet sturdy structure also serves as a support for circuit boards, cables that carry

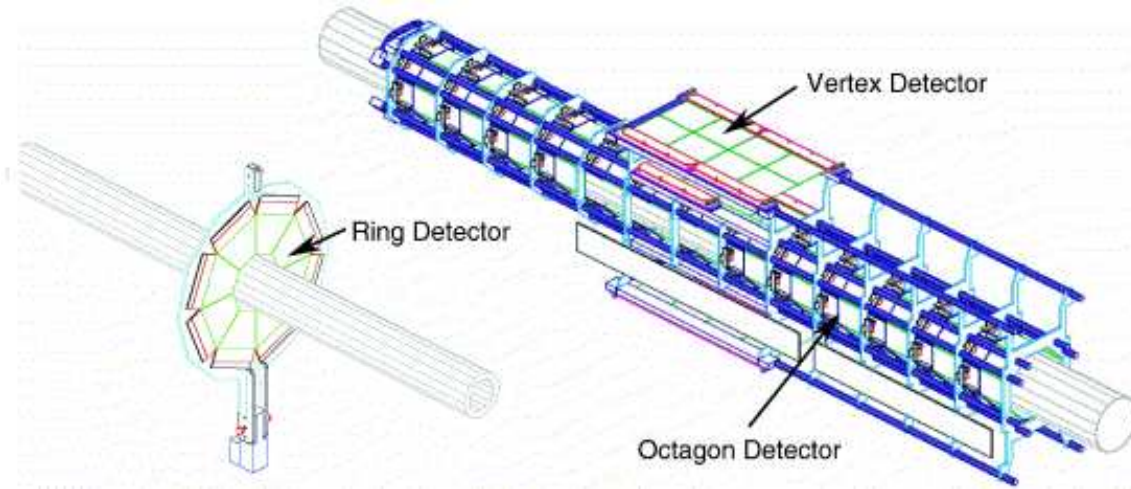


Figure 3. The Octagon Detector (right), also showing the Vertex Detector (above and below) the support frame. The left figure shows a Ring Detector module surrounding the beam-pipe.

signals from the detectors to the rest of the read-out electronics and also the support for the bi-layer Vertex detectors (not discussed here).

In Figure 4, a sample of data has been collected using the Octagon detector. The first two minimum ionizing particles (MIPs) that pass through one detector sensor can clearly be seen as the two peaks.

1.4.3 Silicon Ring Detector

The pseudo-rapidity region covered by the multiplicity array is increased by the Ring Detectors consisting of six octagonal arrays of identical silicon pad detectors. Each Ring is made of eight trapezoidal shaped silicon pad sensors each with eight rows and columns of sensors. Due to the trapezoidal shape, the sizes of the pads vary from $10.2 \text{ mm} \times 10.2 \text{ mm}$ (largest

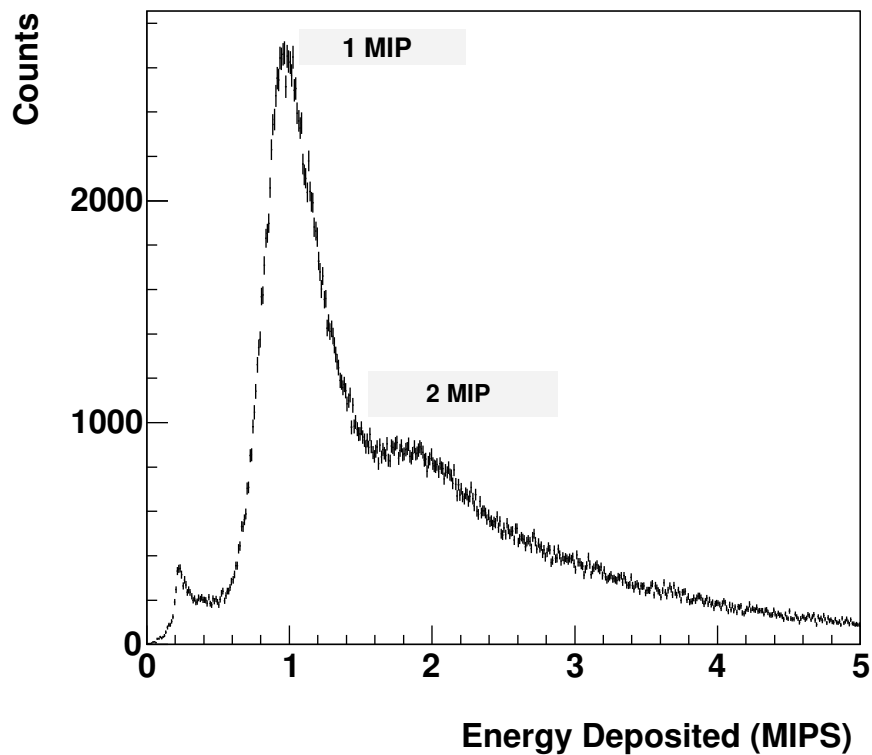


Figure 4. Sample of Energy Deposition Signal seen by the Octagon detector.

radii) to $3.8 \text{ mm} \times 5.1 \text{ mm}$ (smallest radii). These dimensions were chosen to ensure equal pseudo-rapidity coverage ($\Delta\eta \approx 0.1$ unit) by each pad for a collision near the interaction point. The sensors have a gap of 1 mm between one another, and one complete Ring has an outer diameter of 220 mm with an inner diameter of 100 mm.

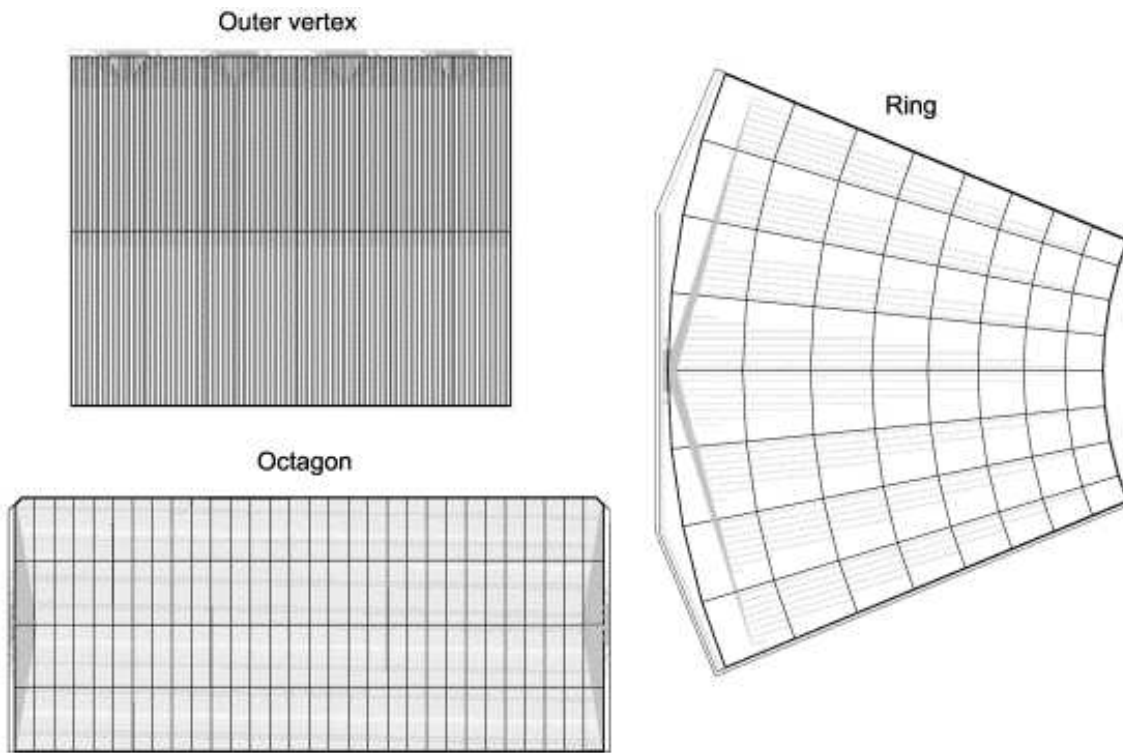


Figure 5. Schematic Layout of the Silicon Sensors used in PHOBOS. The Outer Vertex Detector is not discussed.

The signal from a Ring is read out by a 64-channel preamplifier. A light-weight carbon-fiber frame has a two-fold purpose: to support the weight of the Ring and also to support the circuit boards that carry the signal from each module to the cables and for read-out. The carbon-fiber material is advantageous for this purpose since low- Z material will have a smaller influence on particles travelling out towards other Rings and trigger detectors than a high- Z material would.

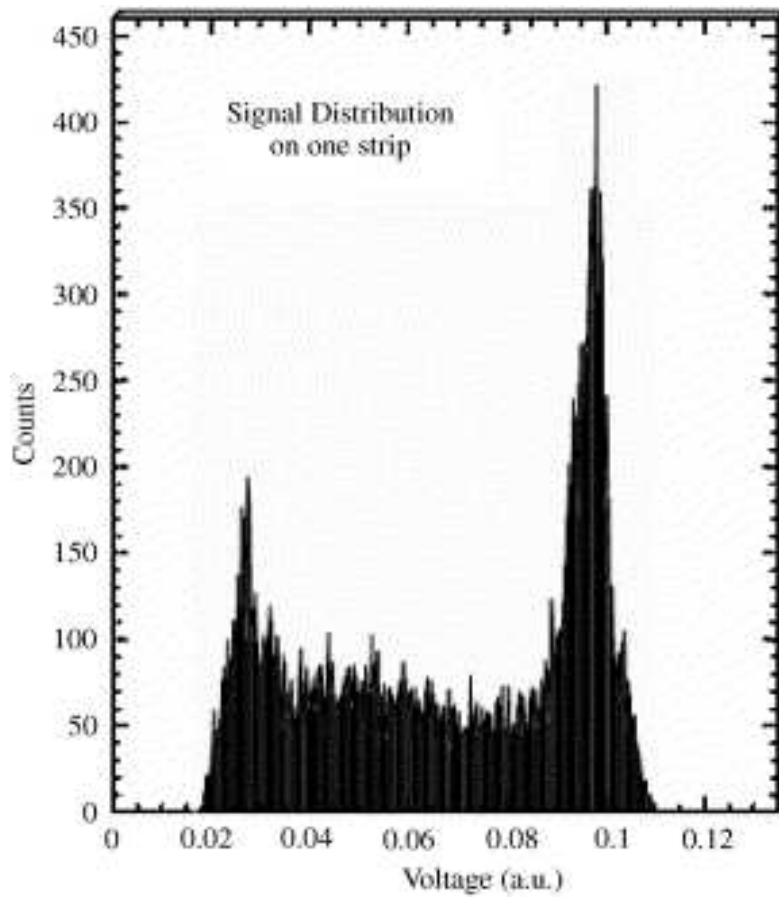


Figure 6. Ring signal distribution from Sn^{113} source.

Figure 6 shows a sample signal distribution of one pad of the ring counter using a Sn^{113} source.

1.4.4 Paddle Trigger Counters

The PHOBOS detector relies on the Paddle counters for primary event trigger decisions. The other trigger detectors are the Time-zero Čerenkov counters (T0), the Zero Degree Calorimeters (ZDC). The latter two will not be discussed in my analysis.

The Paddle counters are made of BC-400 plastic scintillator, arranged in two planar arrays, comprised of 16 detectors (slats) each. The Paddles are located at $z=\pm 3.21$ m away from the interaction point and perpendicular to the beam axis (Figure 2). The Paddles offer pseudo-rapidity coverage in the region $3.2 < \eta < 4.5$. The Paddle detectors are used to determine event centrality by requiring that a certain number of Paddles to be hit and/or a certain energy to be deposited in the Paddles. One example of a simple trigger configuration would be the reduction of background events, by requiring an event to have more than one hit in each Paddle array within a certain time frame. This simple trigger requirement also constrains the interaction to occur in the region between the Paddles. The trigger requirements can be increased in complexity depending on the quality and/or quantity of data required.

CHAPTER 2

PILE-UP

2.1 What is Pile-up?

When the process of reading out the signals from particle detectors includes events resulting from more than one beam interaction, the events begin to accumulate, or “pile-up”. Pile-up is a potentially serious problem for PHOBOS, as collisions occur quite frequently in the interaction region. A peak luminosity of $15 \times 10^{26} \text{ cm}^{-2} \text{ s}^{-1}$ is provided by RHIC, such that collisions occur at a rate of approximately ten thousand per second¹ and $108 \mu\text{s}$ between collisions. From this, it is clear that the read-out for a given event could also contain information from an unrelated physics event. This poses a potentially serious background problem.

In an attempt to combat the problem, a logical path was devised and implemented within the PHOBOS trigger system. There are two intervals in time, with respect to an actual triggered event, that PHOBOS is concerned with: pre-pile-up (an event that occurred before the current event) and post-pile-up (an event that occurs after the current event).

2.1.1 The Importance to PHOBOS

The importance of pile-up to the PHOBOS experiment manifests itself in many ways. Any measurements depending upon the detailed amount of energy deposited can be greatly affected by pile-up. Pile-up can adversely affect the energy deposited for a single event by inflating

¹in the case of the Gold-Gold PR04 data

energy values that could lead to registering an additional hit or a double hit which is not concerned with the current event. Another essential PHOBOS parameter that is possibly affected by pile-up is centrality. This is dependent upon signals from the Paddle detectors. If pile-up leads to inflated signals in the Paddles then, consequently, centrality measurements will be inaccurate.

2.1.2 Pre-Pile-Up

The pre-pile-up check was devised to look over a time interval of $5 \mu\text{s}$ before an actual event. If an unrelated event within this time period were registered in the Paddles, the pre-pile-up logic would record a TRUE. The time interval of $5 \mu\text{s}$ is solely dependent on the read-out properties of the silicon and various electronics used in those detectors. During read-out of the silicon, an output signal is sent to a storage capacitor which will rise to its maximum value in 0.5 to $1 \mu\text{s}$. The time constant for this circuit element is on the order of μ -seconds, and so the signal will decay much more slowly compared to the input. See the *middle* row of Figure 7 for a schematic diagram.

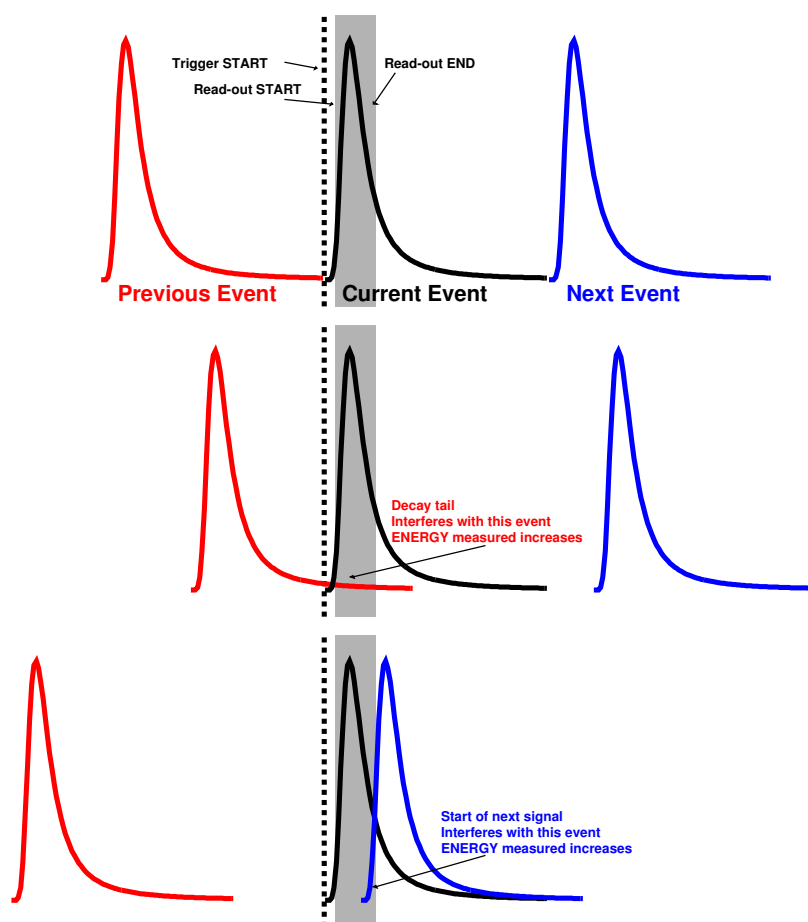


Figure 7. Schematic illustration of pile-up. The *upper* set of plots represent the ideal case of the silicon reading out with no influence from the previous or next event. The *middle* row illustrate a previous event influencing the current event (i.e. Pre-Pile-up). The *lower* row shows the next event influencing the current event (i.e Pre-Pile-up)

2.1.3 Post-Pile-Up

The post-pile-up check is similar to the pre-pile-up check in that it searches for a second signal, in this case *after* the good event. For PHOBOS, the time is $0.6 \mu\text{s}$ and is, again, completely determined by the read-out time of the silicon detectors. Without this check it would be possible for the signal from an unrelated event to influence the signal of a preceding real event. See the *lower* row of Figure 7 for a schematic diagram.

2.2 Pile-Up Trigger Logic

To check for pile-up events during normal data taking runs, a logical path was created. This particular design was implemented to address the various timing conditions that must be taken into consideration, discussed above. Here, only the Pre-Pile-up trigger logic is discussed. The Post-Pile-up trigger logic is similar with small, yet essential, changes and discussed in section 2.2.2. For the complete PHOBOS Trigger Logic diagram, see Appendix B.

2.2.1 Pre-Pile-up Trigger Logic

The logic used for Pre-Pile-up determination is illustrated in Figure 8. In an effort to simplify the explanation of the logic, the design has been broken into two parts: Current Event Processing and Previous Event Processing.

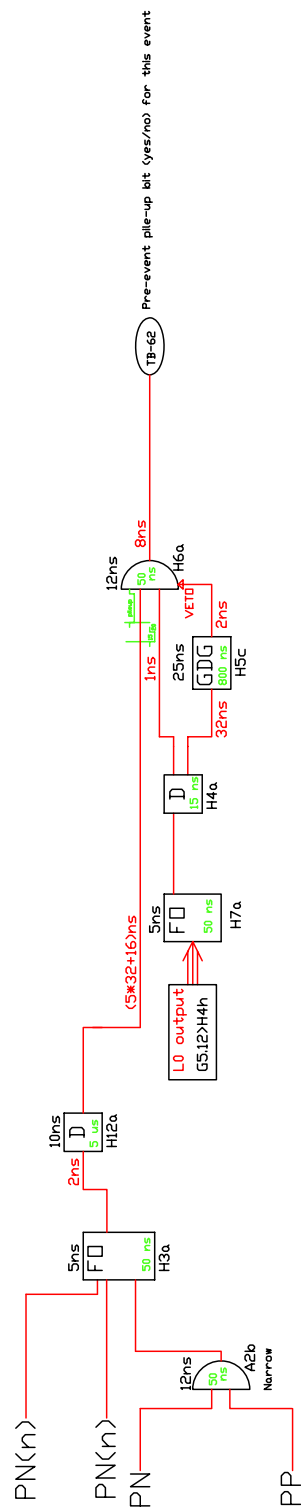


Figure 8. The PHOBOS Pre-Pile-up Trigger Logic Diagram.

2.2.1.1 Previous Event Processing

The *left* side of Figure 9 displays the components responsible for this part of the Pre-Pile-Up check. The inputs of the fan-out (FO) are $PP(n)$ and $PN(n)$ along with an AND of PP and PN which all refer back to the Positive (PP) or Negative (PN) Paddle detectors. The difference between $PP(n)$ and PP is that $PP(n)$ requires n slats to be hit, with the same holding true for $PN(n)$ and PN . During PHOBOS running, n is set at a value of $n > 8$ slats hit. The fan-out integrates all incoming signals over a 5 ns time and emits a pulse with a gate width of 50 ns. This pulse is then sent over a 2 ns cable to a discriminator where the signal is given a gate width of 5 μ s. This outgoing pulse width is one of the critical points in the design and is dependent on the read-out time of the silicon (see section 2.3.2). The pulse is then sent to the AND where it awaits signals from the Current Event Processing.

2.2.1.2 Current Event Processing

Running in parallel to the Previous Event Processing is the logic responsible for processing Current Event. The *right* side of Figure 9 illustrates the design. Initially, a signal from the Level Zero (L0) output (events that have successfully passed the L0 trigger requirements) is split by a fan-out module. One output from the fan-out is sent to the Post-Pile-up check (discussed below), whilst the other is sent to a discriminator. The discriminator creates two 15 ns output signals with one going to a Gate Delay Generator (GDG). This module delays the signal by 25 ns creating a veto to the final AND. The veto ensures that the L0 signal is not the same event simultaneously counted by the Paddle detectors. The veto effectively provides a clean signal to the AND gate. The second signal from the discriminator is sent directly to the AND.

2.2.1.3 Pre-Pile-up Decision

The results from the Current and Previous Event Processing are sent to an AND. If signals from the Current Event Processing are received within the gate of the Previous Event Processing ($5 \mu s$), then the current event is determined to be a pile-up event of the previous event and returns a TRUE statement to a trigger bit. However, if the Current Event and Previous Event do not coincide within the gate time, the Current Event is not a pile-up event, and a FALSE statement results. In this case, the Previous Event is a good event.

2.2.2 Post-Pile-up Trigger Logic

The logic used for Post-Pile-up determination is illustrated in Figure 10. Once again, in an attempt to be unambiguous, the post-pile-up trigger logic can be viewed as two separate logic paths, Current Event Processing and Next Event Processing, that couple to make the final Post-Pile-up decision.

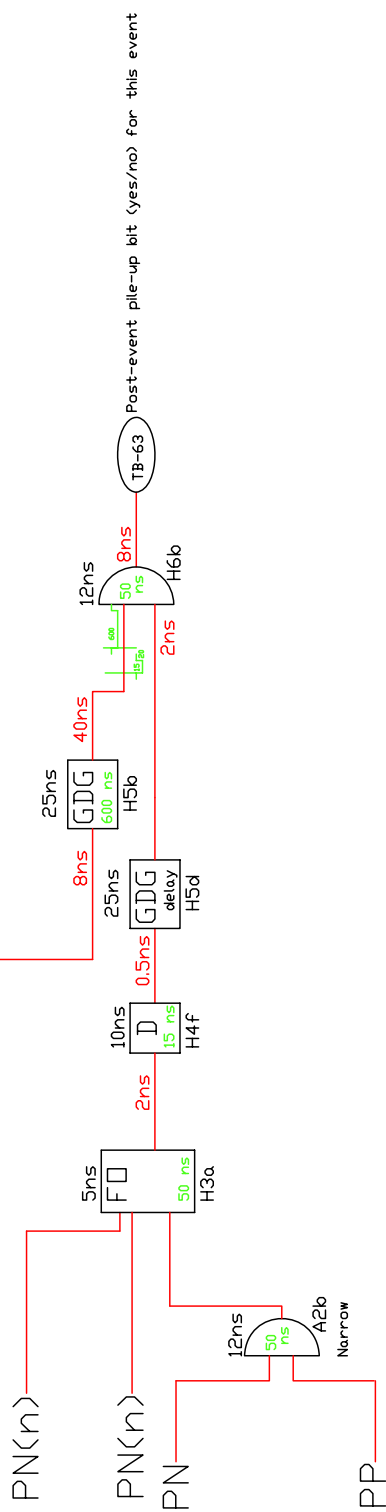


Figure 10. The PHOBOS Post-Pile-up Trigger Logic Diagram.

2.2.2.1 Current Event Processing

The parts of the logic responsible for processing a current event originate at the same point as the Previous Event Processing in the Pre-Pile-up logic. As shown on the *left* of Figure 11, a signal from the Level Zero (L0) output (events that have successfully passed the L0 trigger requirements) is split by a fan-out module and then moves to a Gate Delay Generator. A 600 ns output signal is sent to an AND where it awaits a signal from the Next Event Processing.

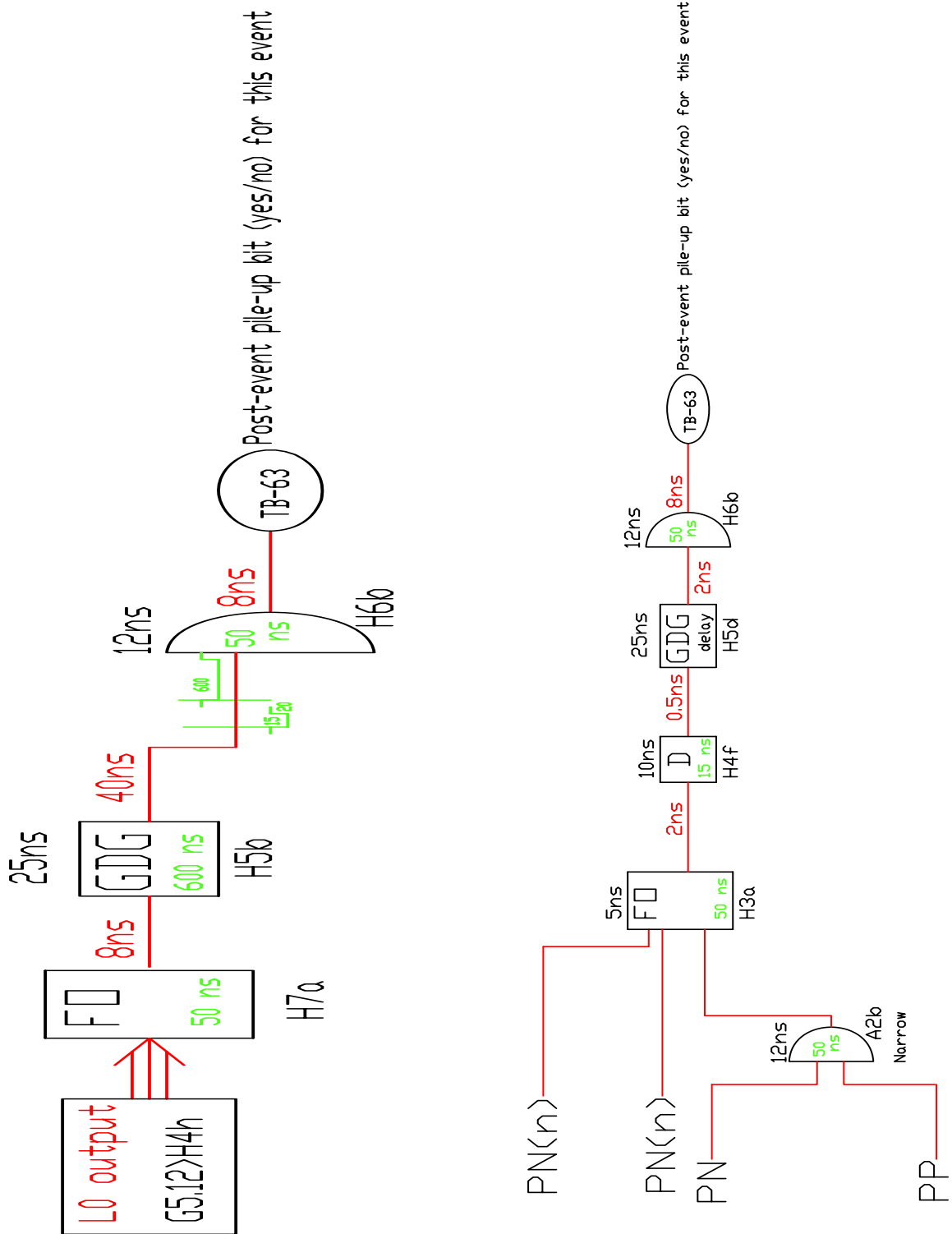


Figure 11. Details of the Post-Pile-up Logic. The *left* illustrates the processing of the Current Event. The *right* shows the logic for processing the Next Event

2.2.2.2 Next Event Processing

Simultaneous processing of the next event originates with the Paddle Detectors as shown on the *right* of Figure 11. The inputs of a fan-out are PP(n) and PN(n) along with an AND gate of PP and PN. The fan-out integrates all incoming signals over a 5 ns time. The fan-out module then produces a pulse with a gate width of 50 ns which is sent over a 2 ns cable to a discriminator. The signal is modified by the discriminator to have a gate width of 15 ns. This pulse moves to a Gate Delay Generator where a 0.6 μ s delay is added to the signal. The output is then sent to the AND gate, where a decision on Post-Pile-up is made.

2.2.2.3 Post-Pile-up Decision

The results from the Current and Next Event Processing are sent to an AND gate. If signals from the Current Event Processing are received within the gate of the Next Event Processing (0.6 μ s), then the Next Event is determined to be a pile-up event of the Current Event and returns a TRUE statement to a trigger bit. However, if the Current Event and Next Event do not coincide within the gate time, the Next Event is not a pile-up event, and a FALSE statement results. In this case, the Current Event is a good event.

2.3 Effects of Pileup on Detectors

In order to determine the overall effect of pile-up in PHOBOS, the signals of the Paddle Detectors, Octagon and Rings were studied.

2.3.1 Paddle Detectors

The Paddle Detectors characteristically have a fast read-out time, due to the scintillator properties and the photomultiplier tubes having a short rise/fall time. Figure 12 is a screen

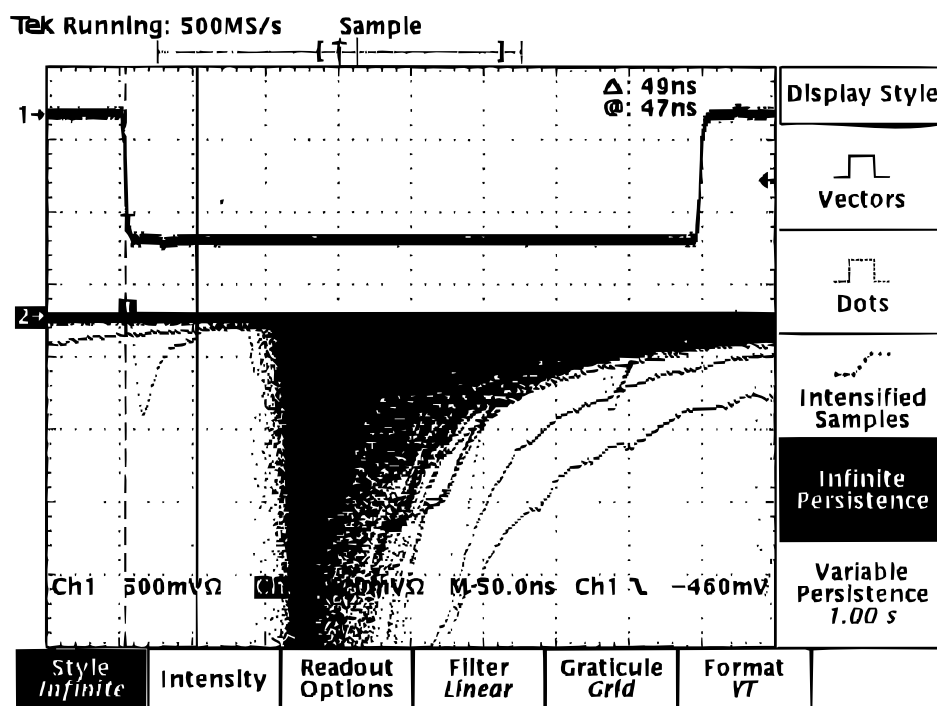


Figure 12. Raw signals from the Paddle Detector. The rise/fall time is approximately 350 ns. The gate width is approximately 400 ns. Each division represents 50 ns.

capture of many saved raw Paddle signals. The rise/fall time is short (≈ 350 ns). For this reason, the effect of pile-up is expected to be minimal.

2.3.2 Octagon

Since the Octagon detectors are silicon based, there is a much greater rise/decay time associated with the read-out of these detectors. Figure 13 is a signal from a silicon detector illustrating the relatively fast rise time, and the much slower decay time, giving a complete

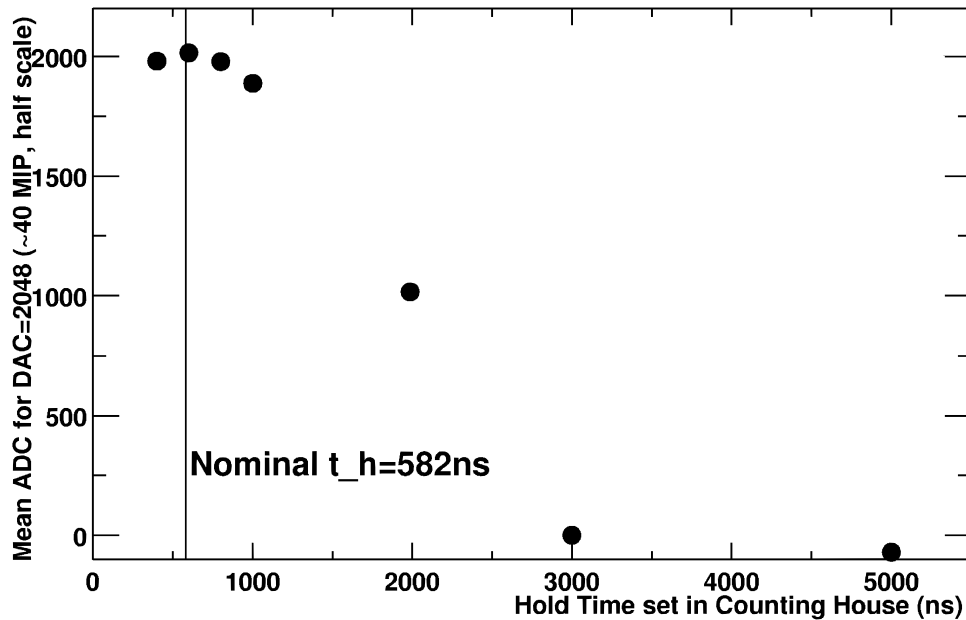


Figure 13. An energy signal from the Octagon silicon detector with time. The rise/fall time is approximately $5 \mu\text{s}$. The y -axis is the energy deposited in the detector, and the x -axis is the Hold Time. Also shown is the amount of time (582 ns) at which the signal is latched in the ADC.

rise/fall time of $\approx 5 \mu\text{s}$. As a result of this large time, the effects of pile-up could be far more apparent with silicon detectors than with the Paddle detectors.

2.3.3 Rings

The Ring Detectors are another silicon based detector, and thus could be more sensitive to pile-up. Also, because of their relatively far distance from the nominal interaction point and their perpendicular arrangement to the beam axis, the Rings are far more susceptible to beam-gas interactions which contributes to pile-up.

CHAPTER 3

STUDY OF PILE-UP

A systematic study of Pile-up was suggested by Richard Hollis at UIC. Please see his UIC Doctoral dissertation (1) for an initial look at pile-up.

3.1 Rationale

In order to determine the effect of pile-up on PHOBOS data, the Paddle MIPs, hits and Paddle Mean variables from the Paddle Detectors were initially considered. These signals are considered first with data containing the pile-up check, and then again for data without the pile-up check. By taking a ratio of the two data sets, the impact of pile-up on the Paddle Detectors will be known.

To investigate the effect of pile-up on the Octagon and Ring Detectors, two signals, EOct and ERing are used. The signals represent the sum of all the individual sensor signals from their respective detectors and are also angle corrected. The EOct and ERing signals are coupled with centrality cuts based on the Paddle Mean signals and are used to determine if the mean value of the EOct or ERing (with and without pile-up) changes, indicating a possible influence from pile-up.

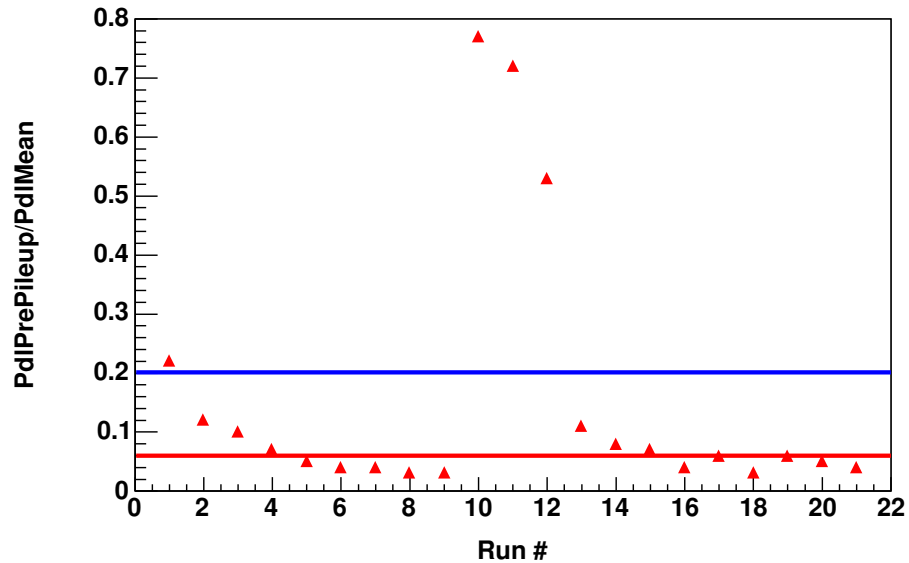


Figure 14. The Ratio (Pile-up/No Pile-up) correlated with Run #. To combat low statistics, three groups were made: 0-6% (below the red line), 6-20% (below the blue line) and 20-80% (above the blue line). These runs are linked during further analysis. The Run #'s correlate back to PR04 run numbers in Table 1.

3.2 Data Used

The data used for this study was obtained from the PHOBOS PR04 Au+Au 200 GeV runs. Samples of data spanning the beginning, middle and end of the complete run were chosen. Within this group, some data were taken during high background (high pile-up) running.

3.2.1 Problem with Statistics

In order to combat the problem of low statistics, the fraction of Pre-pile-up events to non-pile-up events (see Table I) were correlated against each run, as shown in Figure 14. The different runs were then grouped according to this fraction as 0-6%, 6-20% and 20-100%. The runs that fell into these groups were then combined in software for the rest of the study.

It should be noted that only runs in the highest fraction group (20-100%), correspond to data taken during high background running.

Number	Run	Events	Pile-up Events	Ratio (Pile-up/No Pile-up) Events
1	13533	32606	7091	0.22
2	13684	6801	802	0.12
3	13685	63824	6562	0.10
4	13855	22146	1656	0.07
5	13856	67689	3322	0.05
6	13857	25557	1034	0.04
7	13858	37795	1378	0.04
8	13859	76841	2573	0.03
9	13860	37875	1143	0.03
10	13942	94	72	0.77
11	13943	758	545	0.72
12	13944	2239	1176	0.53
13	14218	61572	6734	0.11
14	14220	70728	5711	0.08
15	14221	28028	1923	0.07
16	14222	16365	634	0.04
17	14224	61572	3588	0.06
18	14225	66177	1767	0.03
19	14328	1792	102	0.06
20	14329	4168	190	0.05
21	14330	5521	211	0.04

TABLE I

THE RUNS USED IN THIS STUDY WITH AMOUNT OF NO PILEUP EVENTS, PILE-UP EVENTS AND THE RATIO (PILE-UP/NO PILE-UP).

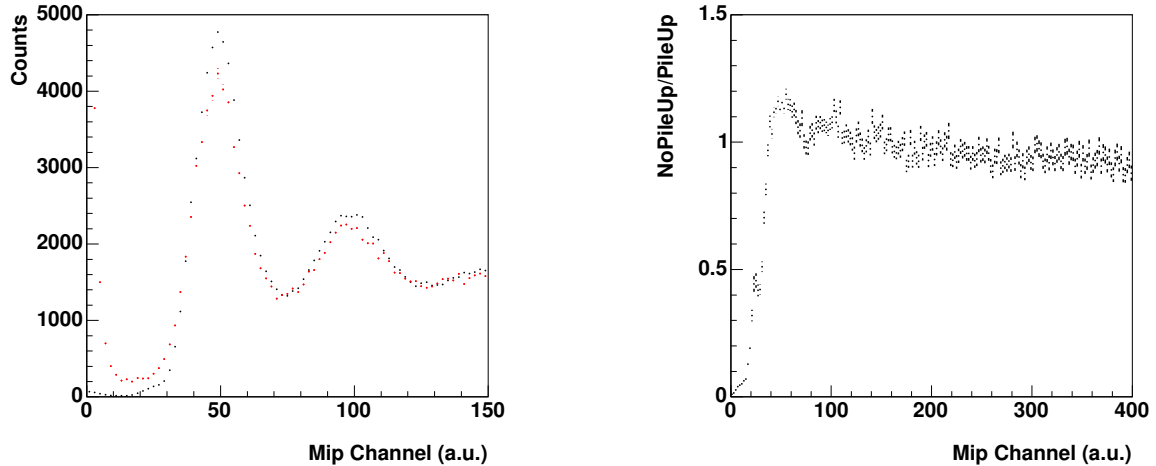


Figure 15. The effect of pile-up on the Paddle’s MIP signals. The *left* illustrates pile-up events (red) with no pile-up events (black). The *right* side shows the ratio of (no pile-up/pileup)

3.3 Study of Pile-up with Paddle Detector

3.3.1 The Effect of Pile-up on MIP signals

The individual MIP signals can be examined individually. For a single run, the raw MIP signals with and without pile-up, are shown on the *left* side of Figure 15, with the 1-MIP signals aligned to a fiducial peak of 50 ADC units above the pedestal. There are a larger number of events triggered with an energy below 25 ADC for pile-up events than without pileup. The width of the MIP signal is also seen to be increased from the no pile-up value of 9.37 ± 0.04 to 9.91 ± 0.19 .

On the right side of Figure 15, the ratio of no pile-up to pile-up shows that the only significant change occurs in the lower part of the energy spectrum.

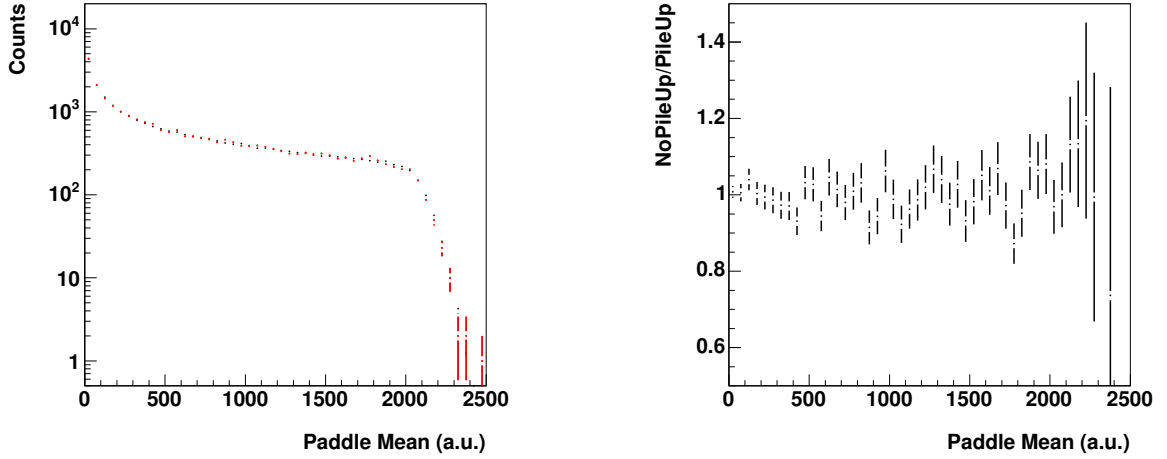


Figure 16. The *left* illustrates Paddle Mean signals (normalized by total number of events) with pile-up events (red) and no pile-up(black). The *right* side is the ratio of no pile-up/pile-up

3.3.2 The Effect of Pile-up on Centrality

The Paddle Mean signals can be used to determine the effect of pile-up on centrality determination. The *left* panel of Figure 16 shows the Paddle Mean signals for both pile-up and no pile-up cases. In general, no difference can be discerned in the high Paddle Mean region that corresponds to the most central collisions. The *right* side of Figure 16 shows the ratio of Paddle Mean signals with no pile-up events to pile-up events has flat slope. Hence, pile-up should not affect the cross-section cut positions.

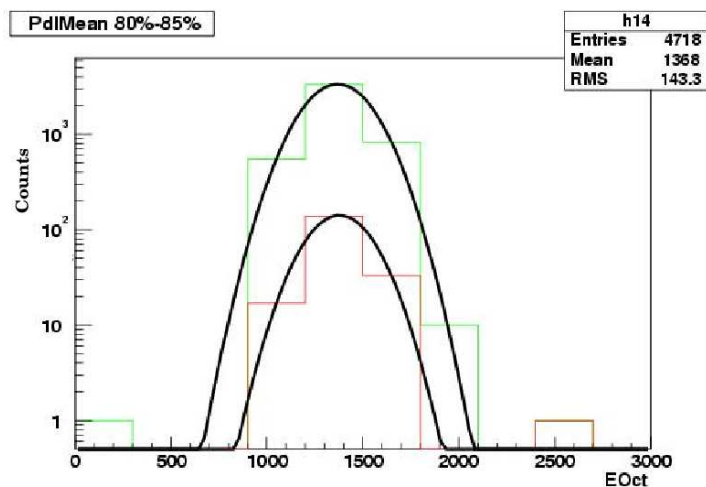


Figure 17. The EOct Signal cutting on the Paddle Mean Signal for the 80-85% centrality with pile-up (red) and without pile-up (green). The mean and sigma values are extracted. In this case, the mean value 1368 for both pile-up and no pile-up, whereas the sigma values are 363 for pile-up and 352 for no pile-up

This last point can be exploited to investigate the effect of pile-up on each unit of centrality. The runs are linked according to the method described in Section 3.2.1. The Paddle Mean signals with pile-up are fitted to a gaussian and the respective mean and sigma values are extracted for each centrality measurement (shown in Figure 17 for the 80-85% centrality bin). The process is repeated for Paddle Mean signals with no pile-up. An example of values for the nine top centrality bin are placed in Table II. It should be noted that the lower centrality bins, the fits become less precise.

Centrality	Pile-up		No Pile-up	
	Mean	Sigma	Mean	Sigma
50 to 55%	354 ± 116	147 ± 152	350 ± 21	150 ± 31
55 to 60%	450 ± 112	123 ± 76	450 ± 32	112 ± 14
60 to 65%	524 ± 108	125 ± 84	542 ± 26	125 ± 24
65 to 70%	679 ± 110	100 ± 69	679 ± 4	88 ± 2
70 to 75%	750 ± 113	103 ± 105	750 ± 18	103 ± 13
75 to 80%	976 ± 110	101 ± 72	979 ± 22	100 ± 14
80 to 85%	1132 ± 121	139 ± 123	1133 ± 24	139 ± 25
85 to 90%	1350 ± 151	120 ± 48	1350 ± 18	152 ± 11
90 to 100%	1765 ± 12	184 ± 11	1789 ± 2	178 ± 2

TABLE II

AN EXAMPLE OF THE MEAN AND SIGMA VALUES WITH ASSOCIATED ERRORS EXTRACTED FROM THE GAUSSIAN FITS FOR THE TOP NINE CENTRALITY BINS.

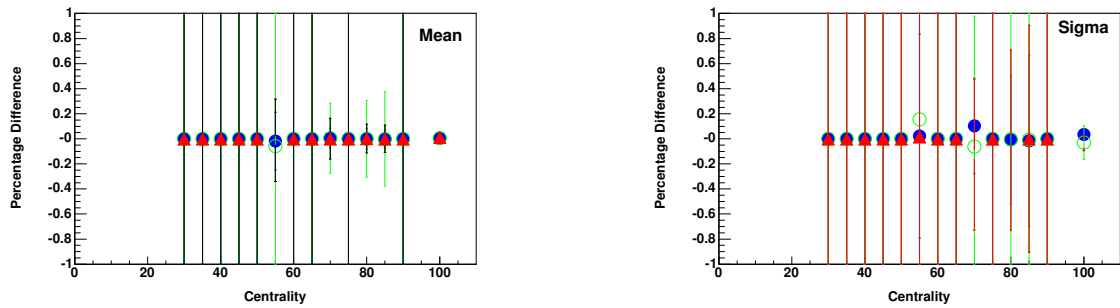


Figure 18. The *left* shows the percent difference in the Mean fit values for pile-up and no pile-up events in the Paddle Mean signals as a function of centrality. The *right* side illustrates the percent difference in the Gaussian sigma fit values for pile-up and no pile-up events in the

Paddle Mean signals as a function of centrality. On both panels, 0-6%(red triangles), 6-20%(blue closed circles) and 20-80%(green open circles). The errors shown arise from the fit parameters.

Figure 18 (*left*) shows the percent difference of the two different Gaussian fit mean values as a function of centrality. Figure 18 (*right*) is the percent difference the Gaussian fit sigma values as a function of centrality. The plots are consistent with a zero slope for each group at each centrality. Errors shown arise from the fit parameters.

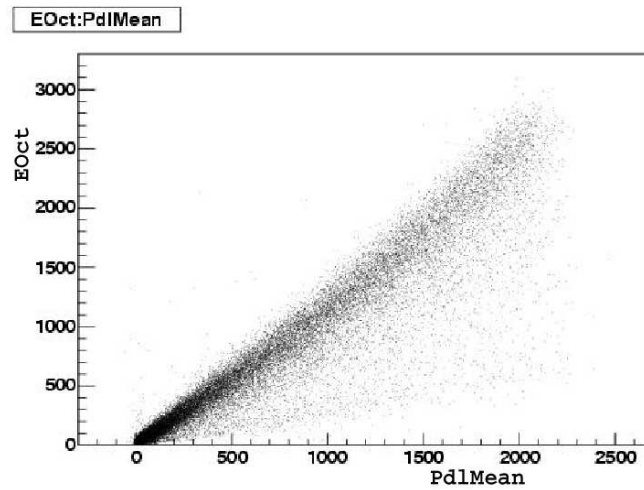


Figure 19. The relationship between the EOct signal and the Paddle Mean signal.

3.4 Paddles Summary

The only region of Paddle signals affected by pile-up is the low energy spectrum as shown by the comparison of the MIP information. There is no statistically significant effect of pile-up on the centrality determination (via PdlMean).

3.5 Study of Pile-up with Octagon Detector

Figure 19 shows the EOct signals correlated with the PdlMean signal, they are monotonically related. Since the Paddles seem to be not significantly affected by Pile-up, it is possible to cut on the PdlMean signals and investigate the effect on the Octagon detector.

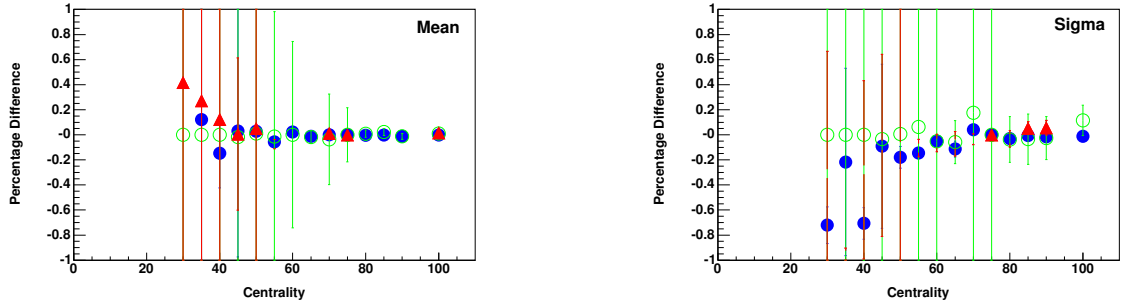


Figure 20. The *left* shows the percent difference in the Mean fit values for pile-up and no pile-up events in the EOct signals as a function of centrality. The *right* side illustrates the percent difference in the Gaussian sigma fit values for pile-up and no pile-up events in the EOct signals as a function of centrality. On both panels, 0-6%(red triangles), 6-20%(blue closed circles) and 20-80%(green open circles). The errors shown arise from the fit parameters.

Once again, the various runs are combined and the EOct signal with pile-up are fitted to a gaussian and the respective mean and sigma values are extracted for varying PdlMean regions (giving centrality regions). The process is repeated for the EOct signals with no pile-up.

Figure 20 (*left*) shows the percentage difference of the two different EOct mean values as a function of centrality. Figure 20 (*right*) shows the percent difference of the sigma values as a function of centrality. The plots are consistent with a zero slope for each group at every centrality measurement. The errors shown are manifested from the fit parameters.

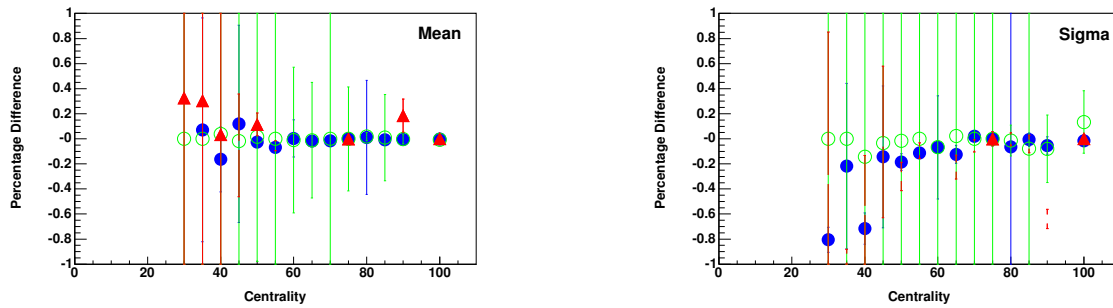


Figure 21. The *left* shows the percent difference in the Mean fit values for pile-up and no pile-up events in the ERing signals as a function of centrality. The *right* side illustrates the percent difference in the Gaussian sigma fit values for pile-up and no pile-up events in the ERing signals as a function of centrality. On both panels, 0-6%(red triangles), 6-20%(blue dots) and 20-80%(green circles). The errors shown arise from the fit parameters.

3.6 Study of Pile-up with Ring Detector

Finally, the effect of pile-up on the Ring Detectors can be investigated in a similar fashion as for the Octagon Detector.

The various runs are linked and the ERing signals for both pile-up and no pile-up are fitted to a Gaussian with the respective mean and sigma values being extracted for varying cuts on the PdlMean signal (centrality regions).

Figure 21(*left*) shows the percent difference of the two different ERing mean values as a function of centrality. Figure 21 (*right*) shows the percent difference in the fit sigma values as a function of centrality. The plots are consistent with a zero slope for each group at every centrality measurement. The errors shown are manifested by the fit parameters.

3.7 Summary of Octagon and Ring Detectors

The maximum effect on the mean of EOct and ERing is 1/2 %. This percentage of pile-up can affect the measurements of multiplicity and jet correlations. The maximum effect on the sigma value for EOct and ERing is 1 %. This measurement of pile-up can affect fluctuation analyses and the resolution of the reaction plane (for measurements of flow).

CHAPTER 4

CONCLUSION

Pile-up plays a very important role in PHOBOS physics measurements. Any measurement which is based on the amount of energy deposited in a detector could be affected.

While the high energy spectrum of the Paddle counters do not seem to be affected by pile-up. However, the low energy spectrum is. The measured effect is not large enough to have any influence on the centrality determination.

The Octagon and Ring silicon detectors are affected by pile-up in a similar way. The maximum effect measured on the mean and sigma values is 1/2 % and 1 % respectively.

Although these numbers are quite small, it is possible that small effects due to pile-up may be seen in measurements of multiplicity, and flow.

APPENDICES

Appendix A

THE PHOBOS COLLABORATION

B.B.Back¹, M.D.Baker², M.Ballintijn⁴, D.S.Barton², R.R.Betts⁶, A.A.Bickley⁷, R.Bindel⁷, W.Busza⁴, A.Carroll², Z.Chai², V.Chetluru⁶, M.P.Decowski⁴, E.García⁶, T.Gburek³, N.George², K.Gulbrandsen⁴, C.Halliwell⁶, J.Hamblen⁸, I.Harnarine⁶, M.Hauer², C.Henderson⁴, D.J.Hofman⁶, R.S.Hollis⁶, R.Holyński³, B.Holzman², A.Iordanova⁶, E.Johnson⁸, J.L.Kane⁴, N.Khan⁸, P.Kulinich⁴, C.M.Kuo⁵, W.T.Lin⁵, S.Manly⁸, A.C.Mignerey⁷, R.Nouicer^{2,6}, A.Olszewski³, R.Pak², C.Reed⁴, C.Roland⁴, G.Roland⁴, J.Sagerer⁶, H.Seals², I.Sedykh², C.E.Smith⁶, M.A.Stankiewicz², P.Steinberg², G.S.F.Stephans⁴, A.Sukhanov², M.B.Tonjes⁷, A.Trzupek³, C.Vale⁴, G.J.van Nieuwenhuizen⁴, S.S.Vaurynovich⁴, R.Verdier⁴, G.I.Veress⁴, E.Wenger⁴, F.L.H.Wolfs⁸, B.Wosiek³, K.Woźniak³, B.Wysłouch⁴

¹ Argonne National Laboratory, Argonne, IL 60439-4843, USA

² Brookhaven National Laboratory, Upton, NY 11973-5000, USA

³ Institute of Nuclear Physics PAN, Kraków, Poland

⁴ Massachusetts Institute of Technology, Cambridge, MA 02139-4307, USA

⁵ National Central University, Chung-Li, Taiwan

⁶ University of Illinois at Chicago, Chicago, IL 60607-7059, USA

⁷ University of Maryland, College Park, MD 20742, USA

⁸ University of Rochester, Rochester, NY 14627, USA

Appendix B

PHOBOS TRIGGER LOGIC DIAGRAM

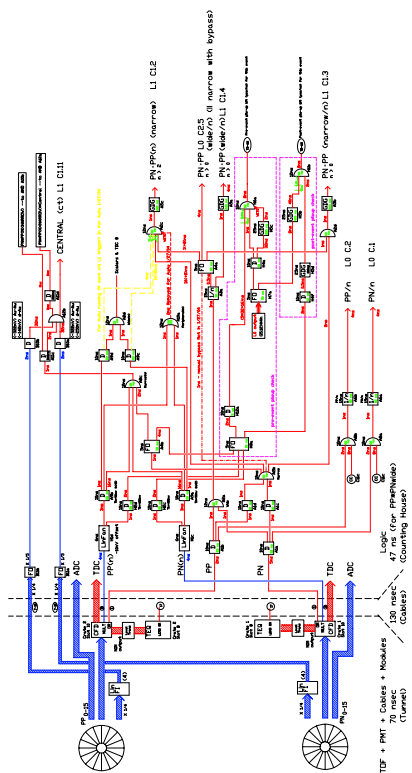


Figure 22. The complete PHOBOS Trigger Logic Diagram for PR04 data taking.

CITED LITERATURE

1. Hollis, R.: Centrality Evolution of Charged-Particles Produced in Ultra-Relativistic $Au + Au$ and $d + Au$ Collisions. Doctoral dissertation, University of Illinois at Chicago, 2005.
2. Noucier, R. et al.: Silicon Pad Detectors for the PHOBOS Experiment at RHIC. Nucl. Inst. Meth. A, 461:143–149, 2001.
3. Pernegger, H.: Layout and Tests of Silicon Pad Detectors for the PHOBOS Experiment at RHIC. Nucl. Inst. Meth. A, 419:549–555, 1998.
4. Back, B. et al.: The PHOBOS Perspective on Discoveries at RHIC. Nuclear Physics A, 757:28–101, 2005.
5. Back, B. et al.: The PHOBOS Detector at RHIC. Nucl. Inst. Meth. A, 499:603–623, 2003.
6. Bindel, R. et al.: Array of Cherenkov Radiators for PHOBOS at RHIC. Nucl. Inst. Meth. A, 488:94, 2002.
7. Bindel, R. et al.: Array of Scintillator Counters for PHOBOS at RHIC. Nucl. Inst. Meth. A, 474:38–45, 2001.
8. Ludlam, T. and McLerran, L.: What Have We Learned From the Relativistic Heavy Ion Collider? Physics Today, 56:48, 2003.

VITA**Ian Kevin Harnarine****Current Address:**

Department of Physics
University of Illinois at Chicago
845 West Taylor Street
Chicago, IL
60607
USA

E-mail: iharna1@uic.edu

Phone: (312) 355-3809

Fax: (312) 996-9016

Personal Information:

Birth Place: Toronto, Canada

Date of Birth: October 28, 1978

Education

Master of Science Program in High Energy Nuclear Physics

University of Illinois at Chicago, Chicago IL 2002-Present

Bachelor of Science in Physics and Astronomy

York University, Toronto, Canada 1997-2002

Research and Experience

Research Assistant-Department of Physics 2004 to Present

University of Illinois at Chicago, Chicago, IL

Teaching Assistant-Department of Physics 2002 to 2004

University of Illinois at Chicago, Chicago, IL

Research Assistant-Department of Physics & Astronomy 1999 to 2002

York University, Toronto, Canada

Summer Student-ZEUS Collaboration Summer 2001

Deutsches Elektronen Synchotron, Hamburg, Germany

Awards and Honors

International Student Service Award 2004

Ontario Scholar 1998